

FOREIGN OBJECT DETECTION BASED ON CIRCULAR BISTATIC SYNTHETIC APERTURE RADAR

Mojtaba Mohammadpoor^{1,2}, Raja S. A. Abdullah^{2, *}, Alyani Ismail³, and Ahmad F. Abas²

¹Wireless and Photonic Networks Research Centre, Faculty of Engineering, Universiti Putra Malaysia (UPM), Selangor 43400, Malaysia

²Islamic Azad University, Gonabad Branch, Iran

³Department of Computer and Communication Systems Engineering, Faculty of Engineering, Universiti Putra Malaysia (UPM), Selangor 43400, Malaysia

Abstract—Synthetic Aperture Radar is well known for producing a radar image of the ground, so it can be used for detecting on-the-ground object which is interesting for some applications. A possible application can be Foreign Object Detection (FOD), which is an important issue in aviation safety. A ground-based Circular Bistatic Synthetic Aperture Radar (Circular-BiSAR) is introduced in this paper. The circular movement makes it more practical while the bistatic configuration offers some advantages. Wideband Linear Frequency Modulated (LFM) chirp pulses are employed here, for transmission and reception of reflection pulses to and from the under test object. A simulated model is developed for the system which analyzes the transmitting, receiving, Doppler and LFM signals by considering the distances and movement of antennas. A prototype system is launched, and some experiments are done to detect and localize various objects based on their reflection properties of microwaves. A processing algorithm is proposed in this paper to confirm the detection. The results show that the proposed system can detect and localize on-the ground objects with as small a dimension as 2 cm height and 2 cm diameter located several metres away.

Received 24 June 2012, Accepted 31 October 2012, Scheduled 27 November 2012

* Corresponding author: Raja Syamsul Azmir Raja Abdullah (rsa@eng.upm.edu.my).

1. INTRODUCTION

Radar has a variety of applications, and detecting on the ground objects may be one of them. One such application is Foreign Object Detection (FOD) for airport runway scanning. The need for an efficient FOD system is a major concern for the aviation industry since the presence of a small object can jeopardize the safety of an aircraft. FODs impose a direct loss around 3–4 billion US dollars per year globally [1]. A radar system is preferable for this application due to its larger coverage area, robustness in poor weather conditions as well as its ability for twenty-four hours operation [2].

Synthetic Aperture Radar (SAR) is a well-known technique for taking high resolution pictures of the ground [3]. Air and space-borne SAR has attracted interest for many years [4]. Recently, the techniques have successfully extended to ground-based SAR (GB-SAR); mostly, GB-SARs are used for extracting geophysical and interferometric information [5].

Bistatic SAR, on the other hand, expands the application of SAR because the redundancy due to spatial separation provides flexibility, improves its ability to detect lower Radar Cross Section (RCS) objects and allows for a sensing system with high reliability, flexibility and resolution [6–8].

Most of SAR systems have a linear movement trajectory; however, there are also some researches in Circular-SAR systems where the airborne radar rotates around the area under surveillance. The rotation increases the aspect angle interval and allows collecting data from different angles [9–11]. These models suffer from practical limitations for ground-based applications. This limitation can be solved by the model presented in [12], where the radar movement exhibit a half-circular trajectory which its centre is out of the scanning area. The ability of this system is shown by detecting objects.

Considering the above-mentioned limitations, this paper proposes a Ground-based Circular Bistatic Synthetic Aperture Radar (Ground-based Circular-BiSAR) which is capable of detecting and localizing small objects. To achieve this, the scheme employs a Wideband Linear Frequency Modulated (LFM) chirp pulses as transmitting signal. The advantages of using LFM include their higher signal-to-noise ratio and less hardware complexity compared to short impulses [13]. LFM signals can be generated using different methods, based on desired applications [14]. The received pulses at the radar are then passed onto a processing algorithm which has been proposed in this paper.

In the first part of the paper, a theoretical model is developed for the system, following by series of field experimentation using a

prototype. The result indicated that the proposed system can detect and localize objects as small as 2 cm high and 2 cm diameter located several metres away. With the usage of lower frequencies, the system may also be suitable for other applications such as mine detection and through the wall detection applications.

In order to cover a wide area as an airport runway, a series of the proposed system may be used. In the commercial front, some FOD detection systems, such as Tarsier@ [2], are already in the markets which are mentioned to be effective in object detection at relatively far distances. However, a complete comparing the proposed systems by them is left to the future, when the proposed system be matured enough specially in terms of detecting far objects. However, the proposed system has some advantages over existing methods. Using SAR idea in this way offers some advantages to the system. Utilizing a bistatic topology makes it flexible to be distributed to cover bigger areas and detect lower RCS objects. In addition, it uses centimetre-waves instead of millimetre waves, which is used by most of the commercial systems. Using low frequencies offers the system several advantages, for example being more robust against harsh environmental conditions, such as rain, fog and snow, running in a more costly manner, and being usable for applications that may need wave penetration, such as buried or behind-obstacles object detection.

The rest of this paper is organized as follows. The Circular-BiSAR will be introduced in detail in Section 2, followed by modelling and simulating parts in Section 3, and experimental aspects of the system in Section 4. Both simulation and experimental signals' characteristics will be analyzed in Section 5, and The Detection and localization algorithm will be proposed in Section 6. The images of the area, as the output of proposed algorithms will be shown in Section 7. The paper will be concluded in Section 8.

2. GROUND-BASED CIRCULAR-BISAR SYSTEM

The proposed LFM Circular-BiSAR system consists of a transmitter antenna installed on an arm which rotates slowly around a tower to scan a 180° swath. A receiver antenna is installed on another tower near to the receiver. A train of pulses is being sent continuously, and their reflections are recorded for further processing. Fig. 1 shows the layout of the proposed system for ground object detection.

The used signal for the proposed radar system is Linear Frequency Modulated (LFM) pulses. A LFM pulse can be formulated as follows [4, 9]:

$$p_T(t) = \text{rect}(t/T_p) \exp(j\beta t + j\alpha t^2) \quad (1)$$

where T_p is the pulse duration and α the chirp rate. The instantaneous frequency of the chirp, which is the derivative of its phase respect to time, can be measured as:

$$IF = \frac{\partial}{\partial t} (j\beta t + j\alpha t^2) = \beta + 2\alpha t, \quad 0 \leq t \leq T_p \quad (2)$$

As it is shown, the chirp frequency sweeps from β to $\beta + 2\alpha T_p$ in the pulse duration; hence the carrier frequency can be evaluated as:

$$F_C = \beta + \alpha T_p, \quad (3)$$

And its baseband bandwidth is defined as:

$$BW = \alpha T_p \quad (4)$$

The chirp bandwidth depends on the chirp rate and pulse duration. Fig. 2 shows an apt illustration of a theoretical transmitted signal during the experiment.

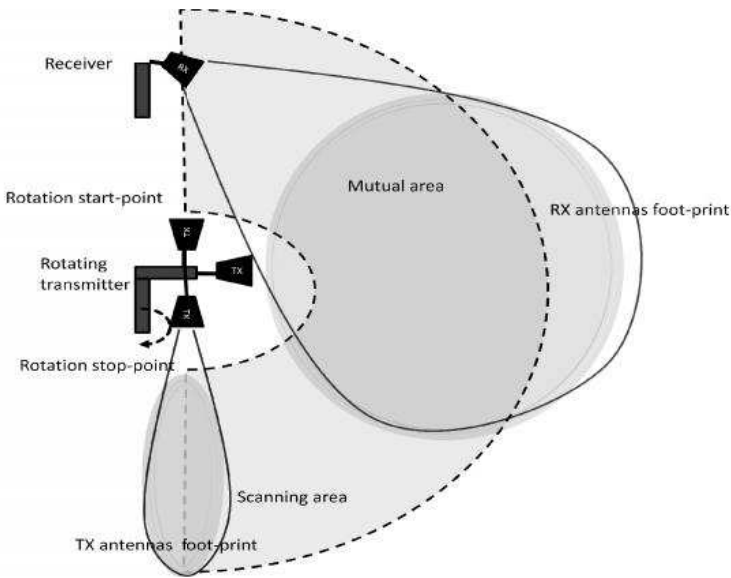


Figure 1. The layout of circular-BiSAR.

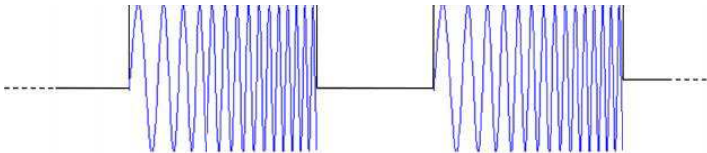


Figure 2. Transmitted LFM signal.

Table 1. System characteristics in circular-bisar.

Bandwidth	1.5 GHz
Carrier frequency	6.75 GHz
Chirp duration	10 ms
Chirp rate, α	1.5×10^{11} Hz/s
Pulse Repetition Interval	40 ms
Sampling frequency	50 kHz
Scanning time	52.180 s
Antennas heights	1.7 m
Antennas distances	5.25 m

In the experiment, the chirp pulse sweeps from 6 GHz to 7.5 GHz in 10 ms, and it is repeated for every 40 ms. The characteristics of the system and transmitted signal are tabulated in Table 1.

2.1. Pulse Compression

When the object is illuminated by the transmitted signals from the radar, the reflected signals received at receiver exhibit identical shape to the original signal; the only differences are their amplitudes and time delays. The amplitude of the chirp pulse also depends on the position of the antenna which rotates at a very slow speed, so it can be considered as a function of slow time ' τ '. Thus the transmitted LFM pulse can be represented as:

$$p_T(t) = a(t, \tau) \exp(j\beta t + j\alpha t^2) \quad (5)$$

Based on the stop-and-go assumption, the pulse will illuminate the object and reflect back to the receiver within a time limit where the instantaneous change in position can be neglected. Hence, the received pulse can be considered as follows:

$$p_R(t) = a(t - t_d, \tau) \sigma \exp(j\beta(t - t_d) + j\alpha(t - t_d)^2) \quad (6)$$

where ' σ ' represents the Radar Cross Section (RCS) of the object. ' t_d ' is the time delay which can be expressed as $t_d = (R_T + R_R)/c$, where R_T , R_R , c are the transmitter and receiver ranges and speed of light, respectively. By using the homodyne receiver and neglecting the effect of t_d in the envelop of the pulse (i.e., the video pulse), the resultant

signal will be as:

$$\begin{aligned}
 p_T(t)*p_R(t) &= \frac{\sigma a(t, \tau)^2}{2} \cos[2\pi(\beta t + \alpha t^2)] \cos[2\pi(\beta(t-t_d) + \alpha(t-t_d)^2)] \\
 &= \frac{\sigma a(t, \tau)^2}{2} \{ \cos[2\pi(\beta t + \alpha t^2) + 2\pi(\beta(t-t_d) + 2\pi\alpha(t-t_d)^2)] \\
 &\quad + \cos[2\pi(\beta t + \alpha t^2) - 2\pi(\beta(t-t_d) - 2\pi\alpha(t-t_d)^2)] \} \quad (7)
 \end{aligned}$$

Here, the first sinusoidal signal has high frequency because α and β are normally very big values in comparison to t_d . The second low frequency term and its harmonics can be filtered by using a low-pass filter, which will reduce the Equation (7) to:

$$\begin{aligned}
 p_{rec}(t) &= \frac{\sigma a(t, \tau)^2}{2} \cos[2\pi(\beta t + \alpha t^2) - 2\pi(\beta(t-t_d) - 2\pi\alpha(t-t_d)^2)] \\
 &= \frac{\sigma a(t, \tau)^2}{2} \cos[2\pi(2\alpha t_d t + \beta t_d - \alpha t_d^2)] \quad (8)
 \end{aligned}$$

Note that this is a frequency modulated and phase modulated signal with $2\alpha t_d$ frequency and $\beta t_d - \alpha t_d^2$ time delay. Therefore, by measuring its frequency and knowing α , the value of t_d can be evaluated.

Using LFM pulses has some advantages. Firstly, it helps in achieving high detection capability of a long pulse while retaining the range resolution of a narrow pulse. Secondly, LFM pulses significantly reduce hardware complexity, for example sampling frequency [13]. Bandwidth of the signal affects the range resolution of the system. The range resolution of the system in direction of slant range can be measured as $\delta_R = \frac{c}{2B}$, where c is speed of light and B is the bandwidth of the signal. By using the LFM specification illustrated in Table 1, due to having a wideband signal (i.e., 1.5 GHz) the system is capable of distinguishing between the objects of 10 cm difference in range.

3. CIRCULAR-BISAR MODELLING

A simulated model of the proposed system is needed for further processing. Doppler frequency has already been derived for 2D view in [15], and in this paper it will be evaluated in a 3D view of the proposed system as shown in Fig. 3. The XYZ -coordinate system is established so that its origin placed on the transmitter platform 'O'. The height of the antennas and the arm length are shown as ' h ' and ' r '. The squint and grazing angles between the antennas are also shown as ' η ' and ' ξ ' respectively. ' η ' varies by slow-time while ' ξ ' depends on the object range. While the transmitter antenna is rotating, its angle to the x -axis can be represented as a function of slow time ' $\varphi(\tau)$ '.

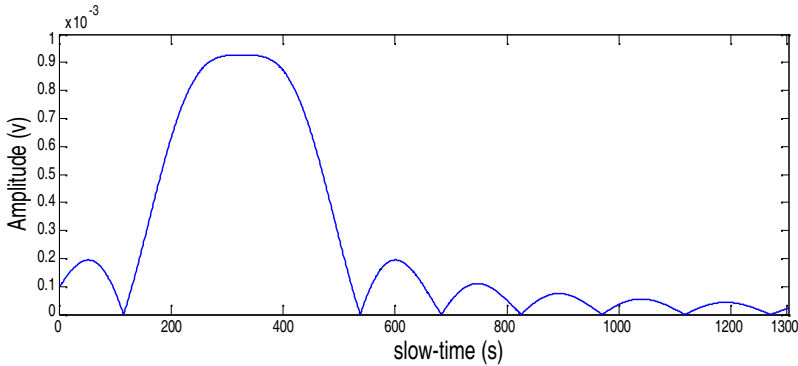


Figure 4. Doppler signal of a point object at 45° .

$\frac{d\varphi(\tau)}{dt}$ is the angular velocity of the rotating transmitter and can be shown as $\Omega(\frac{\text{rad}}{\text{sec}})$, hence:

$$f_D = \frac{1}{\lambda} \frac{r \cdot R_g \cdot \Omega \cdot \cos(\gamma) \sin(\varphi(\tau) - \theta)}{R} \quad (13)$$

In addition to Doppler frequency, the strength of the signal produced by a point object also depends on its range, reflectivity and the solid angle to the antenna. Considering all these parameters as well as antennas tilting angles; the absolute value of Doppler signal when a point object positioned at 45° (respect to x -axis) is shown in Fig. 4. As it has shown, the Doppler signal almost follows the antenna pattern; this similarity can be used as a tool for detecting and localizing the point-object.

4. CIRCULAR-BISAR EXPERIMENTAL SETU

Experimental part is the most important part due to lots of parameters that may affect the system. In this way, a prototype of the proposed Circular-BiSAR is launched over a clear field which is similar to an airport runway. The horn antenna, the arm, and the computer-controlled motor which are the transmitter part, are shown in Fig. 5(a). The receiver antenna which is a horn antenna installed on a tower is shown in Fig. 5(b). A N-type connector which is a metallic cylinder with 2 cm diameter and 2.5 cm height is used as the object, as shown in Fig. 5(c). The object size is selected based on FOD definition [17]. The height of the towers as well as the antennas' angles are adjusted iteratively until the position where the biggest joint-area and strongest reflection from the object are attained.

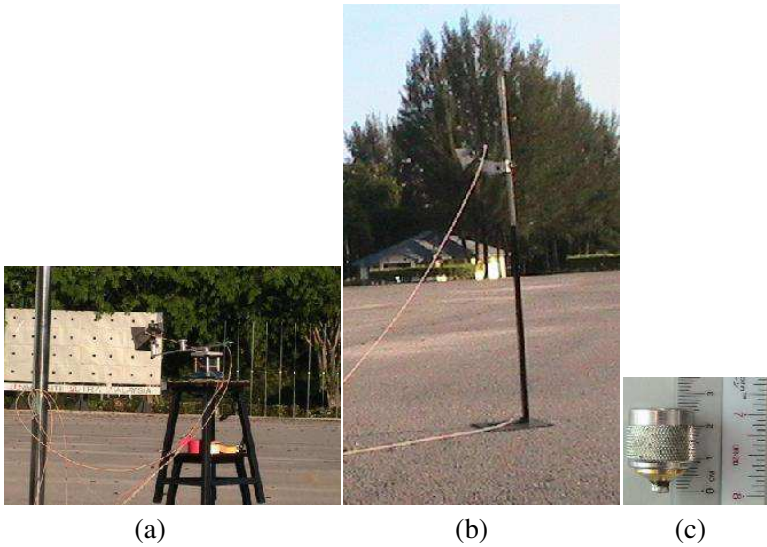


Figure 5. Experimental setup. (a) The transmitter part. (b) The receiver antenna. (c) Object shape.

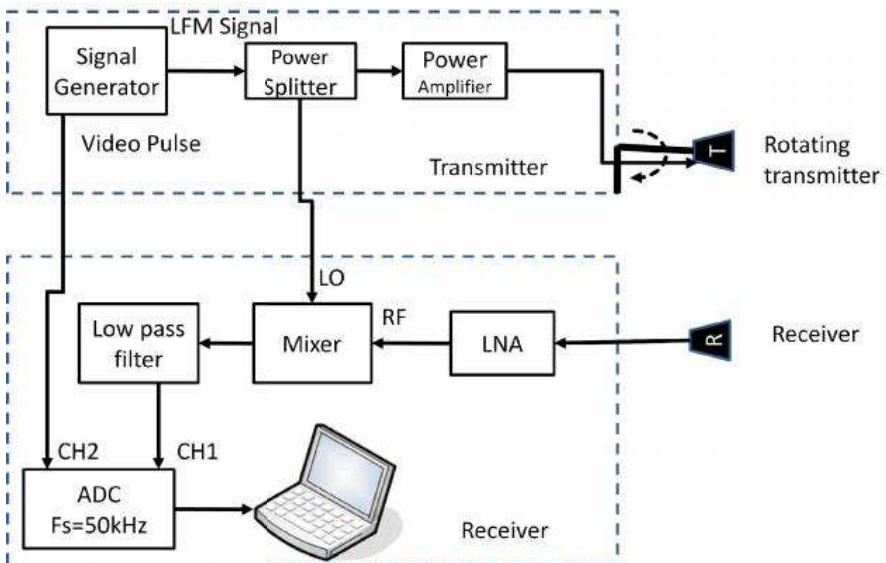


Figure 6. Schematic view of transmitter and receiver circuit.

A schematic circuitry diagram of the transmitter and receiver is shown in Fig. 6. A signal generator is used to generate the LFM pulses. A video pulse (i.e., the envelop of LFM pulses) is also produced which will be used to extract the pulses in a synchronous manner. The LFM output is split into two parts: one part is used for transmitting after amplification, while the other is used as a reference local oscillator in the receiver. The received signal in each receiver is amplified and down-converted using the mixer prior to filtering the high frequencies using the lowpass filter [18].

The mixer, which is a nonlinear device, multiplies the received signal with the reference signal. The output of the mixer comprises of both low frequency and highfrequency parts as shown in Equation (21). By using a LowPass Filter (LPF), the lowfrequency part can be recorded by a low-cost AnalogetoDigital Converter (ADC).

The video pulse in channel 2 is synchronized with the pulse train and can be used to extract the pulses, thereby ensures a coherent signal processing. While receiving this train of pulses, the antennas keep rotating, and hence each pulse carries information about the scanned area at that time instant.

To analyze the system ability in detecting and localizing small objects, a small object is placed at 6.75 m and its angle is 36° respect to the x -axis.

4.1. Frequency-range Calibration

The relationship between range and frequency beat is given by [9] and calculated in Equation (8) where:

$$f_{\text{beat}} = 2\alpha t_d = 2\alpha(R_T + R_R)/c \quad (14)$$

The total time delay of the signal consists of a delay in free space and a circuit delay, including delay in cables, connectors, components, etc.. Thus, Equation (14) can be rewritten as:

$$f_{\text{beat}} = f_{cd} + 2\alpha t_d = f_{cd} + 2\alpha(R_T + R_R)/c \quad (15)$$

where ' f_{cd} ' is the frequency due to circuit delay. ' f_{cd} ' is difficult to be measured, so a more practical formula is used as follows:

$$f_{\text{beat}} = f_1 + \frac{2\alpha}{c}(R_T + R_R - 1) \quad (16)$$

where f_1 is the frequency beat generated by a reference point at 0.5 m slant range from the antennas in a monostatic configuration.

A frequency-range profile for the system can be achieved during the calibration stage. more details about it can be found in [12].

5. SIGNAL CHARACTERISTICS

By concurrently sending the LFM pulse train during the scanning period and recording the received signal, a long-period pulse train signal is acquired. Considering the scanning time and pulse width, the scanning area is divided into $52.180/0.04 \cong 1304$ arcs. In this way, 1304 pulses are recorded. By considering a 180° clockwise rotation about the centre of the antenna as shown in Fig. 2(a), and for 1304 slow time (ST) positions, the first pulse in the train corresponds to $ST = 1$ which is the starting position; the 652nd pulse depicts $ST = 652$, which is the point where the antennas cross the middle line, and the last pulse indicates the stopping position.

In simulation part, the recorded signal can be attained by inserting a single-frequency sinusoidal waveform into the Doppler signal during the pulse width. Its frequency can be calculated by using Equation (8) where R_T is varying by slow-time. Fig. 7 shows a part of theoretical and experimental signals.

As inferred first, the experimental signal does not look like the theoretical one, due to running the experiment in a real field, so the object signal is hidden among infinitive numbers of clutter signals. In order to remove the clutter, the system runs two time, firstly over a clear field, and secondly when the object is placed at its position. Now, the pure object signal can be obtained by clutter removing. A point at 6.75 m range and 45° is selected for analyzing the system and shown as $P1$ through this paper. Fig. 8 shows the theoretical and experimental signals when the object is at $P1$. The amplitudes are normalized to one. The object effect is just appeared in the pulses when it was in the both antennas scene; so $ST = 352$ which is the point that the transmitter antenna faced to the object is selected in Fig. 8. From the range measuring Equation (16), the expected frequency beat, which

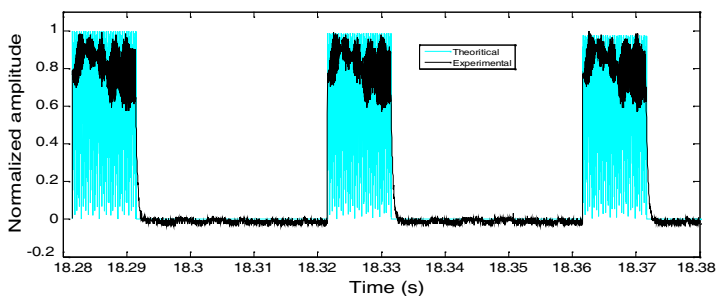


Figure 7. Theoretical and experimental recorded signal in time domain.

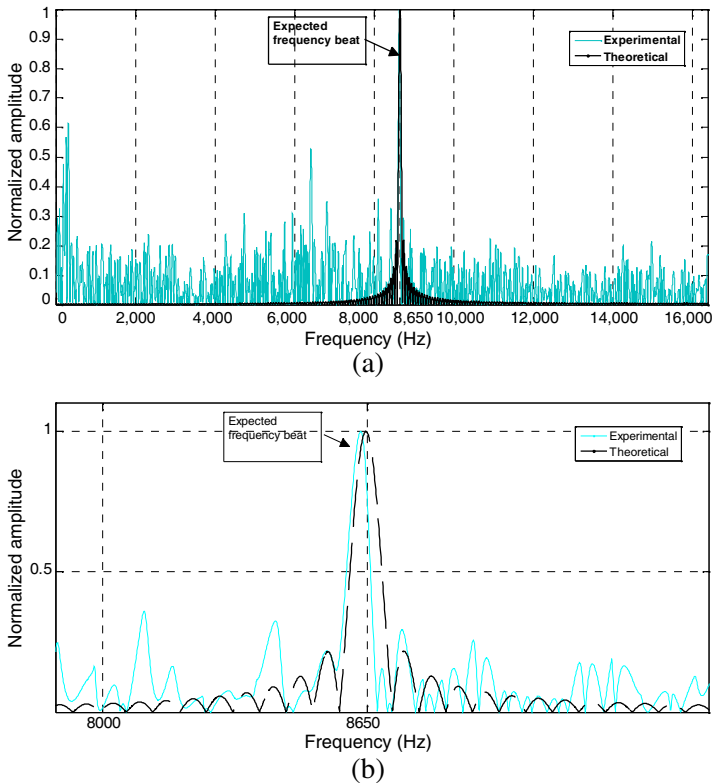


Figure 8. Theoretical and experimental signal when the object is at $P1$. (a) Full span. (b) Zoomed in around the expected frequency beat.

creates by the object at $P1$ position is 8.65 KHz. This is coinciding with simulated and experimental frequency beat shown in Fig. 8.

As shown in Fig. 8, some other peaks may also appear in addition to the object beat. These may be due to thermal noise, quantizing noise, multiplicative noise (i.e., small instability of radar) or even a moving insect or leaf in the area. They will be deleted in the next step when their trend is tracked in different slow-times.

6. CIRCULAR-BISAR SIGNAL PROCESSING

There are several processing algorithms for different SAR and BiSAR systems as shown in [19]. A new processing algorithm for the proposed circular-BiSAR system is proposed in this paper. The algorithm is divided into two parts, which will be discussed in this section.

6.1. Extracting Algorithm

A pre-processing algorithm for extracting the pulses from the pulse train is introduced. The start of each pulse is detected by finding the positive edge of the video pulse signal. A certain length of the signal is recorded based on the pulse duration and sampling frequency. A Hilbert-Huang transform (HHT) [20,21] is applied on the pulse, to filter the DC value. Fast Fourier Transform (FFT) is then applied on the resultant pulse in order to convert it to the frequency domain. The output of the proposed pre-processing algorithm is a matrix with number of rows as the number of pulses in the signal (i.e., 1304 in this case) and number of columns as half of the number of FFT points.

6.2. Detecting and Localizing Algorithm

An algorithm is introduced in this section in order to detecting and localizing the object using data-matrices attained by simulation or by applying extracting algorithm over experimental recorded signal. Range compression is done in the homodyne receiver circuit. Cross-range compression is done in this section by means of matching the object Doppler signal by its equivalent simulated signal.

The resultant matrix, upon applying the extracting algorithm on a clutter signal is a $1304 \times NFFT/2$ matrix. Another matrix with the same dimensions is constructed from the object signal, for instance, when the object is at $P1$. This matrix carries information about the object which is embedded in clutter. The pure object-only matrix can be attained by coherent subtracting the two matrices. This new matrix will be referred as the object matrix in future processing. Its rows represent the different slow-time positions of the antennas. Each column on the other hand, represents the frequency of the iso-range of the object within the vicinity of the antennas. The object signature appears when the object falls within the beam of both antennas, as shown in Fig. 8.

The algorithm calculates the peak positions shown in Fig. 8. The points which their amplitudes are bigger than the noise threshold are considered as candidate frequencies. The noise threshold is changing in each frequency, and it can be defined in the calibration stage as the value created by the smallest detectable object at that frequency.

Each frequency represents a unique summation range by using Equation (16), so by having the beat frequency, $(R_T + R_R)$ is known, which represents an iso-range. From a mathematical point of view, the locus of the points with a constant summation distance $(R_T + R_R = \text{Const})$ from two focal points is an 'ellipse', as shown in 2D in Fig. 9. In this case, the focal points are the transmitter and receiver antennas, so

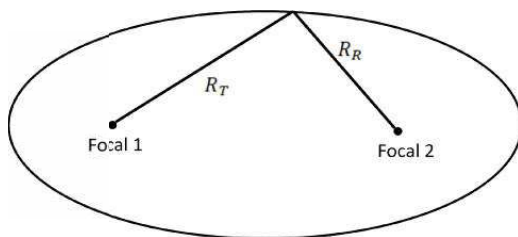


Figure 9. Ellipse definition for two focal points.

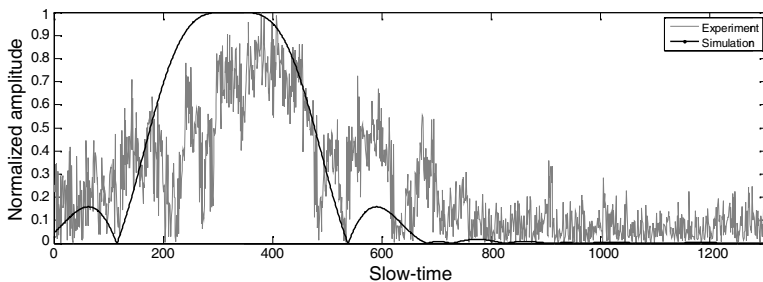


Figure 10. A slice of beat frequency in all slow-times.

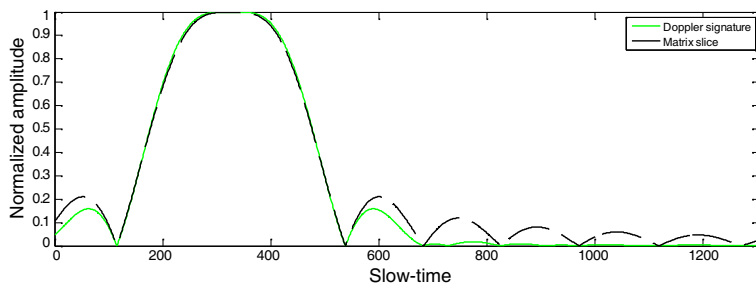


Figure 11. Doppler signature versus matrix column.

the ellipse projection on the ground can be considered as the ground-iso-range.

On the other hand, the candidate frequency values in all slow-times can be approximated as the object Doppler signature; hence it can be used for cross-range analyzing. Fig. 10 shows the column of the data-matrix at the beat frequency. Both experimental and simulation signatures are presented at the same figure. The experimental signature may be smoothed by using different techniques such as taking its envelop, de-noising using wavelet tools or averaging around a small frequency band around the beat frequency. The latter one is due to

this fact that the beat frequency covers a small band.

Instead of the simulated matrix column, the simulated Doppler signature can be used. Fig. 11 compares the Doppler signature by matrix column at beat frequency; as it is shown they are close to each other, especially in bigger amplitudes, where the antenna faces the object.

In order to find the position of the object in slow-time (i.e., the object angle), the signal from the object was compared to the simulated Doppler's signal. Several shifted copies of the Doppler signature in a band of slow-time positions around the peak position are used as reference signals for cross-range imaging technique in circular-BiSAR. Square Euclidean distances between two signals are measured. The summation of all points is considered as the similarity merit, so that its minima represent the matched signal, which is the slow-time position of the object (its angle).

The remaining problem is to clarify the object by knowing the range summation (i.e., iso-range) and angle. As it has shown in Fig. 12, $(R_T + R_R)$, and θ are known. d, h, r are towers distance, height and arm-length, which are known from system configuration. The problem might be simplified as below:

Known parameters:

$$R_T + R_R = A, \quad A \text{ is a known value} \quad (17)$$

$$\theta, d, h, r$$

The problem is finding R_{Tg} .

In order to solve it, the following formulas can be extract by Fig. 12:

$$(R_{Tg} - r)^2 + h^2 = R_T^2 \quad (18)$$

$$R_{Rg}^2 + h^2 = R_R^2 \quad (19)$$

By inserting (18) and (19) in (17), we can have:

$$\sqrt{R_{Rg}^2 + h^2} + \sqrt{(R_{Tg} - r)^2 + h^2} = A \quad (20)$$

$$R_{Rg} = \left\{ \left[A - \sqrt{(R_{Tg} - r)^2 + h^2} \right]^2 - h^2 \right\}^{1/2} \quad (21)$$

Also by evaluating the two triangles created by plotting the normal line from object to base-line, we can obtain:

$$\left[d - R_{Tg} \cos \left(\frac{\pi}{2} - \theta \right) \right]^2 + \left[R_{Tg} \sin \left(\frac{\pi}{2} - \theta \right) \right]^2 = R_{Rg}^2 \quad (22)$$

By inserting R_{Rg} calculated in Equation (21) into Equation (22), a long equation for calculating R_{Tg} will be attained. This equation can be

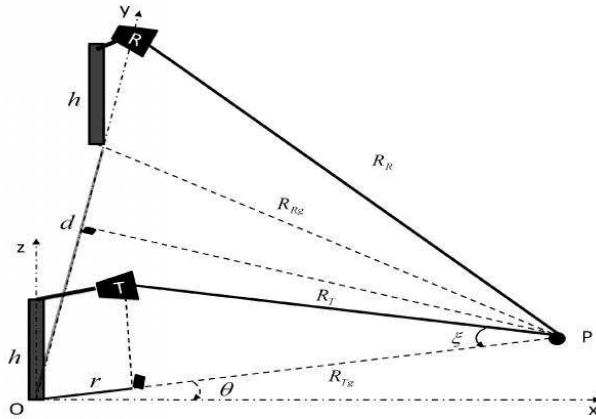


Figure 12. Object localizing after measuring iso-range and angle.

solved using numerical methods and the possible answer in the desired area will be attained. Therefore the position of the object will be defined.

7. CIRCULAR-BISAR IMAGIN

Range processing in circular-BSAR defines the iso-range of the object. By applying the cross-range processing, the iso-Doppler of the object will be known. Iso-range and iso-Doppler curves will grid the scanned area into several cells, as shown in Fig. 13. As illustrated, iso-Dopplers are lines origin from the transmitting source. Iso-ranges, on the other hand, are ellipses where their focal points are transmitter and receiver antennas. The cell-sizes depend on the scanning speed and cell positions. The cross-range resolution of the system depends on the distances of the iso-Dopplers which depend on the rotation speed. The objects used in the experiments are smaller than the cell-sizes and the cross-connection point of iso-range and iso-Doppler is considered as the object position.

In order to generate an image of the area, we can divide the area into plenty of small cells, as shown as the background in Fig. 13. The size of these under-layer cells is considered as $1 \text{ cm} \times 1 \text{ cm}$, to produce a high resolution image of the area. By applying the range and cross-range analysis methods on an experimental data-set, the iso-ranges and iso-Dopplers for each point of the area are defined. Iso-curves will get bigger values at the object position. Therefore, the multiplication of the two iso-curve values is assigned to each under-layer cell of cross-

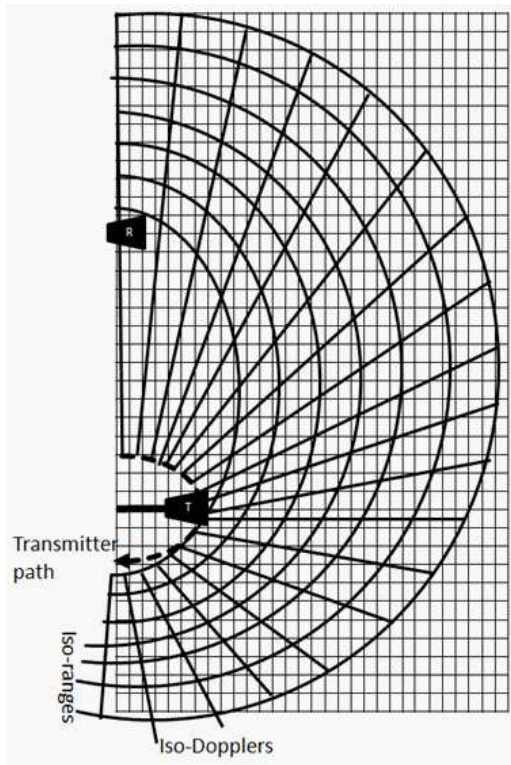


Figure 13. Scanned area gridded into cells.

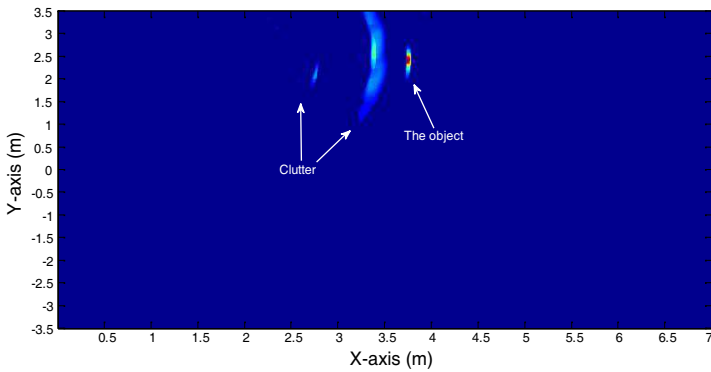


Figure 14. Image of the area where a small object is placed at 6.75 m and 36°.

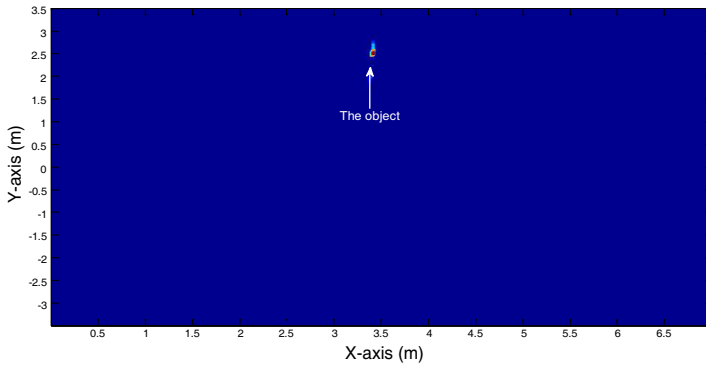


Figure 15. Pure image of the area where a small object is placed at at 6.75 m and 36° .

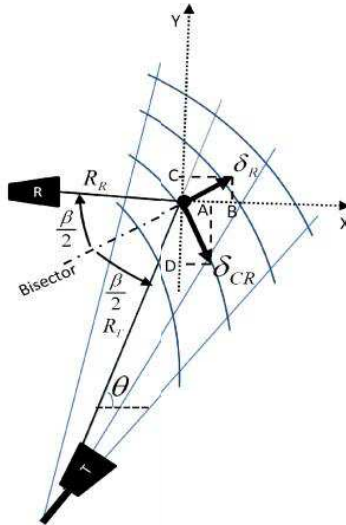


Figure 16. Resolution cells in Cartesian coordinate directions.

connection point of the two curves. Repeating this iteration for all under-layer cells will generate an image of the scanned area. Fig. 14 shows the generated image by analyzing the data-set of scanning the area where an object is placed at 6.75 m and 36° .

As illustrated in Fig. 14, the object is detected. In addition more other objects are also detected. They are environmental objects, hence their positions and values depend on the area. Regarding the application, the main aim is highlighting the foreign object. Therefore,

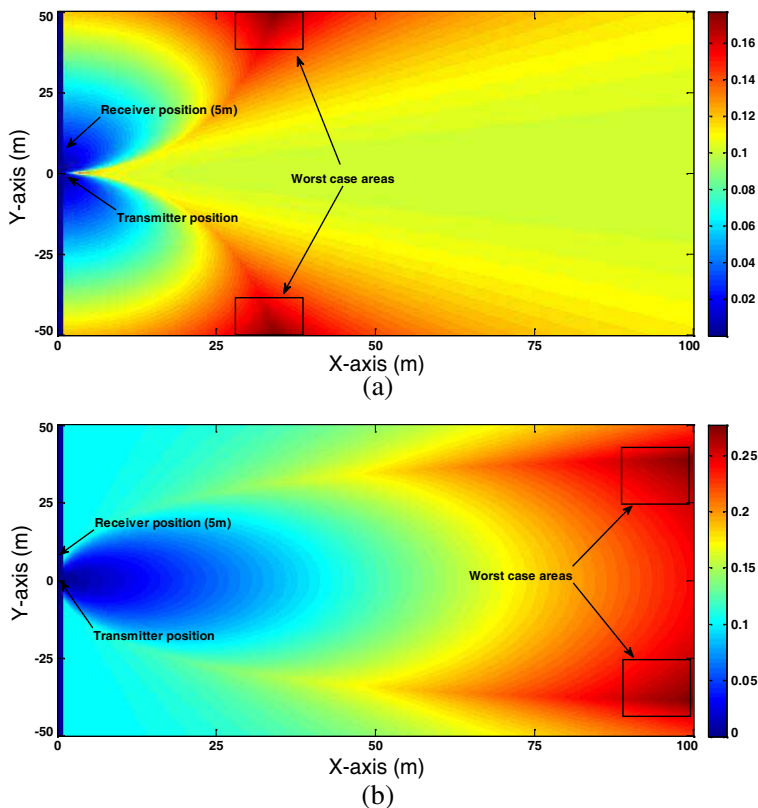


Figure 17. Circular-BiSAR resolution in (a) x -axis direction, (b) y -axis direction.

first the scanning system is launched over the clear area (i.e., without existing the object) to generate a clutter matrix. By this, all existing things are considered as clutter. After throwing the object on the area, the system scans the area again. The clutter matrix is subtracted from data matrix recorded in this step to obtain another data matrix which carries the pure effect of the object. By processing the clutter-removed matrix we can create an image of the area which just shows the object effect. Fig. 15 shows the generated image.

8. SYSTEM RESOLUTION IN CARTESIAN DIRECTION

As explained in Sections 2 and 7, the range and cross-range resolutions are vectors in direction of bisector and iso-range of the system, as shown in Fig. 16 where δ_R , δ_{CR} and β are range and cross-range resolutions

and bistatic angle respectively.

Since the values and directions of them are changing in the space, resolution in Cartesian directions may be helpful to evaluate the system resolution. The resolution in the x -axis and y -axis directions can be calculated as:

$$\delta_X = \min\{|PA|, |PB|\} = \min\{|\delta_R \cos(\theta - \beta/2)|, |\delta_{CR} \sin(\theta - \beta/2)|\} \quad (23)$$

$$\delta_Y = \min\{|PC|, |PD|\} = \min\{|\delta_R \sin(\theta - \beta/2)|, |\delta_{CR} \cos(\theta - \beta/2)|\} \quad (24)$$

Fig. 17 shows the system resolution in x and y directions for an $100\text{ m} \times 100\text{ m}$ area. The positions of the transmitter and receiver antennas are shown and the worst case areas are highlighted. As shown, the worst resolution values will not exceed from 16 cm in x -direction and 25 cm in y -direction.

9. CONCLUSION

Circular-BiSAR, a Ground-based Circular Synthetic Aperture Radar, is introduced in this paper to detect on-the-ground objects. One possible application of the system could be runway FOD detection. Using the system for other possible applications is left for future. The system is first analyzed mathematically, and then a prototype is developed for further experimentation. Here, a transmitter antenna is installed on an arm that rotates slowly about a pivot with the aid of a pc-controlled motor on a tower. A receiver is installed on another tower aligned with transmitting tower. A Linear Frequency Modulated chirp signal with 1.5 GHz bandwidth is used. Several experiments are done to detect a small $2\text{ cm} \times 2\text{ cm}$ cylindrical object at various distances. The received signals are down-converted using a circuit, and then recorded by a computer. A processing algorithm is developed for analyzing the signals and generating an image of the area based on them. From the resultant images, it is found that the proposed Circular-BiSAR system is capable of detecting and localizing even small on-ground-objects located several meters away from the antenna. It can be concluded that the proposed BiSAR system could be a suitable alternative for use as FOD detection systems, after some modifications to increasing its coverage.

REFERENCES

1. Procaccio, F. A., *Effectiveness of FOD Control Measures*, Embry-Riddle Aeronautical University Worldwide Campus, 2008.

2. Patrick, D. L., P. R. D. Beasley, and Q. Qineti, "Tarsier[®], a unique radar for helping to keep debris off airport runways," *The IET Seminar on the Future of Civil Radar*, 2006.
3. Chang, Y.-L., C.-Y. Chiang, and K.-S. Chen, "SAR image simulation with application to target recognition," *Progress In Electromagnetics Research*, Vol. 119, 35–57, 2011.
4. Chen, J., J. Gao, Y. Zhu, W. Yang, and P. Wang, "A novel image formation algorithm for high-resolution wide-swath spaceborne SAR using compressed sensing on azimuth displacement phase center antenna," *Progress In Electromagnetics Research*, Vol. 125, 527–543, 2012.
5. Zhou, Z.-S., W. M. Boerner, and M. Sato, "Development of a ground-based polarimetric broadband SAR system for noninvasive ground-truth validation in vegetation monitoring," *IEEE Transactions on Geoscience and Remote Sensing*, Vol. 42, No. 9, 1803–1810, 2004.
6. Shi, J., X. Zhang, and J. Yang, "Principle and methods on bistatic SAR signal processing via time correlation," *IEEE Transactions on Geoscience and Remote Sensing*, Vol. 46, No. 10, 3163–3178, 2008.
7. Cherniakov, M., "Space-surface bistatic synthetic aperture radar — Prospective and problems," *RADAR*, 2002.
8. Cherniakov, M., Editor, *Bistatic Radar: Principles and Practice*, John Wiley, Chichester, 2007.
9. Soumekh, M., *Synthetic Aperature Radar Signal Processing with MATLAB Algorithms*, John Wiley, New York, 1999.
10. Majumder, U., et al., "Synthetic aperture radar moving target indication processing of along-track monopulse nonlinear gotcha data," *IEEE Radar Conference*, 1–6, May 2009.
11. Yan, W., J.-D. Xu, G. Wei, L. Fu, and H.-B. He, "A fast 3D imaging technique for near-field circular SAR processing," *Progress In Electromagnetics Research*, Vol. 129, 271–285, 2012.
12. Mohammadpoor, M., R. R. Abdullah, A. Ismail, and A. F. Abas, "A circular synthetic aperture radar for on-the-ground object detection," *Progress In Electromagnetics Research*, Vol. 122, 269–292, 2012.
13. Duersch, M. I., "BYU micro-SAR: A very small, low-power, LFM-CW synthetic aperture radar," Master's Thesis, Brigham Young University, Provo, Utah, 2004.
14. Chua, M. Y. and V. C. Koo, "FPGA-based chirp generator for high resolution UAV SAR," *Progress In Electromagnetics*

- Research*, Vol. 99, 71–88, 2009.
15. Abdullah, R. R., M. MohammadPoor, A. Ismail, and A. F. Abas, “A multistatic circular synthetic aperture radar for small object detection,” *IEEE Radar Conference*, Kansas City, MO, USA, 2011.
 16. Willis, N. J., *Bistatic Radar*, SciTech Publishing, 2005.
 17. O’Donnell, M. J., *Airport Foreign Object Debris/Damage (FOD) Detection Equipment*, Federal Aviation Administration, Landover MD., U.S.D.O. Transportation, 2009,
 18. Cherniakov, M, et al., “Automatic ground target classification using forward scattering radar,” *IEE Proceedings — Radar, Sonar and Navigation*, Vol. 153, No. 5, 427–437, 2006.
 19. Sun, J. P., et al., “Extended exact transfer function algorithm for bistatic SAR of translation invariant case,” *Progress In Electromagnetics Research*, Vol. 99, 89–108, 2009.
 20. Huang, N. E. and S. S. Shen, *Hilbert-Huang Transform and Its Applications*, Vol. 5, World Scientific Pub Co Inc., 2005.
 21. Chen, W., R. Chen, and D. Ding, “Application of hilbert-huang transform to MMW doppler radar,” *International Conference on Microwave and Millimeter Wave Technology, ICMMT Proceedings*, April 21–24, 2008.